Microwave Giant Magnetoresistance and Ferromagnetic and Spin-Wave Resonances in (CoFe)/Cu Nanostructures

V. V. Ustinov[a,*], **A. B. Rinkevich**[a,**], **I. G. Vazhenina**[b,***], **and M. A. Milyaev**[a]

[a] *Institute of Metal Physics, Ural Division, Russian Academy of Sciences, Yekaterinburg, 620108 Russia*
[b] *Kirensky Institute of Physics, Siberian Branch, Russian Academy of Sciences, Krasnoyarsk, 660036 Russia*
*e-mail: ustinov@imp.uran.ru
**e-mail: rin@imp.uran.ru
***e-mail: irina-vazhenina@mail.ru
Received January 24, 2020; revised March 23, 2020; accepted March 23, 2020

Abstract—The microwave phenomena that occur in magnetic multilayer (CoFe)/Cu nanostructures, which have a giant magnetoresistance, are studied. The transmission of waves through a nanostructure is used to investigate the microwave giant magnetoresistance effect. The changes in the transmission coefficient at frequencies of 29−38 GHz are found to exceed the relative magnetoresistance, which distinguishes the system under study from the nanostructures studied earlier. Ferromagnetic and spin-wave resonances are used to study the angular dependences of the microwave absorption spectra of a multilayer $(CoFe/Cu)_n$ nanostructure. The following parameters are determined: the critical angle that determines the boundaries of the ranges of excitation of uniform and nonuniform spin modes, the type of boundary conditions describing the pinning of spins on the outer nanostructure surfaces, and the surface anisotropy and exchange interaction constants.

1. INTRODUCTION

Antiferromagnets and artificial structures with antiferromagnetic ordering have specific magnetic properties and, hence, are of deep interest. The works performed under the guidance of A.S. Borovik-Romanov (see, e.g., [1, 2]) are important for understanding the dynamic magnetic properties of antiferromagnets. He studied the antiferromagnetic resonance and spin waves in antiferromagnets and found that the spin waves in antiferromagnets obey a linear dispersion law; in addition, he comprehensively investigated the parametric excitation of spin waves. Among the artificial structures with antiferromagnetic ordering, the metallic nanostructures consisting of ferromagnetic and nonferromagnetic metal layers are of particular interest. In these nanostructures, ferromagnetic metal layers are coupled by exchange interaction and the magnetization in each layer is antiparallel to the magnetization in the neighboring layer. These nanostructures have the giant magnetoresistance (GMR) effect [3, 4], which is caused by the spin-dependent electron scattering by a ferromagnetic layer boundary. The interlayer exchange interaction has an oscillating character depending on the nonferromagnetic layer (spacer) thickness. The GMR effect was observed in such nanostructures at microwave frequencies (μGMR) [5]. The authors of [6, 7] proposed and substantiated a method of microwave passage through a nanostructure as a convenient method to study μGMR. The state of the art in this field of research was comprehensively described in review [8]. In the microwave passage method, a nanostructure sample is placed in the cross section of a rectangular waveguide and the modulus of transmission coefficient as a function of the magnetic field is measured. As was proved in [6, 7], the relative change in the transmission coefficient is equal to the relative magnetoresistance far from ferromagnetic resonance conditions.

The μGMR effect has an important practical application in recording−reading devices and magnetic sensors. For these purposes, nanostructures must have the magnetoresistance as high as possible and the saturation field as low as possible. These properties can be achieved in CoFe/Cu nanostructures, which have the record value of μGMR [9]. The ferromagnetic layer in these nanostructures consists of a CoFe alloy.

Ferromagnetic resonance (FMR) and spin-wave resonance (SWR) methods are known to be reliable instruments for determining the following fundamental parameters of magnetic materials: effective magnetization M_{eff}, exchange interaction constant A inside a layer, spin-wave stiffness η, and surface anisotropy constant K_S. In turn, the angular dependences of the resonance fields for both the perpendicular and parallel orientations of dc magnetic field **H** with respect to

(a)

| PyCr; 3 nm |
| Co$_{88}$F$_{12}$; 1.3 nm |
| Cu; 2.05 nm |
| Co$_{88}$F$_{12}$; 1.3 nm |
| ... |
| Cu; 2.05 nm |
| Co$_{88}$F$_{12}$; 1.3 nm |
| PyCr; 5 nm |
| Ta; 5 nm |
| Corning glass |

(b)

3.0126 μm

3.0059 μm
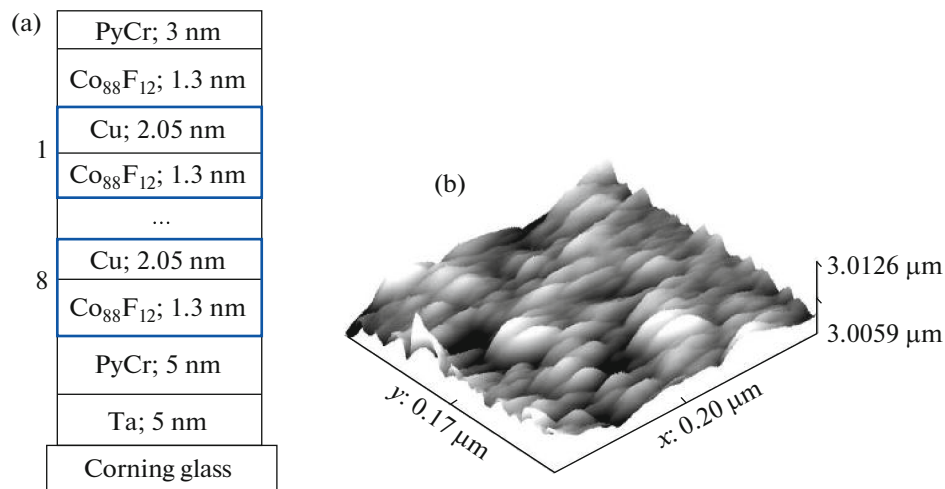
y: 0.17 μm   x: 0.20 μm

Fig. 1. (Color online) (a) Composite structure of superlattice sample 2. (b) Tunneling microscope image of the surface relief of sample 2.

the surface of a thin film can be used to obtain information on the presence and contribution of anisotropy of various types, namely, crystalline magnetic anisotropy, magnetoelastic, and surface anisotropy [10−13].

An analysis of microwave absorption spectra in thin films has to take into account the following factors: boundary conditions [14−17], the ferromagnetic film thickness [18], the composition [19−22], and the structural parameters (thickness, number of layers) [23, 24] of a multilayer film. The rules of numbering the standing spin modes detected in a microwave spectrum were described in detail in [18, 23, 25−28].

Using these factors for analyzing microwave absorption spectra, we were able to reveal a number of main characteristics of the magnetic dynamics of CoFe/Cu nanostructures by μGMR, FMR, and SWR techniques. As objects of inquiry, we chose [Co$_{88}$Fe$_{12}$/Cu]$_n$ superlattices, where the nonmagnetic layer (hereafter, spacer) thickness in one sublattice corresponds to the first maximum of the oscillating dependence of magnetoresistance and that in the other sublattice, to the second maximum. These samples have strongly different saturation fields and magnetoresistances. In addition, we also studied the three-layer Co$_{88}$Fe$_{12}$/Cu/Co$_{88}$Fe$_{12}$ structure. Microwave transmission measurements were carried out in the frequency range 29−38 GHz, and measurements by a resonance spectrometer were carried out at 9.2 GHz. In the next section, we describe the technique of nanostructure preparation and the experimental technique used in this work. The results of studying the μGMR effect and, then, FMR and SWR are then presented.

2. EXPERIMENTAL

[Co$_{88}$Fe$_{12}$/Cu] nanostructures were prepared by magnetron sputtering on an MPS-4000-C6 (Ulvac) setup [29, 30]. Sputtering was performed on Corning glass substrates of thickness $d_s = 0.2$ mm at room temperature and a deposition rate of 6.7 nm/min (Cu) and 2.8 nm/min (Co$_{88}$Fe$_{12}$). The argon pressure was 0.1 Pa and magnetron evaporator power was 100 W. Superlattice samples with the compositions Ta(5)/PyCr(5)/[Co$_{88}$Fe$_{12}$(1.5)/Cu(0.95)]$_{24}$/Ta(5) (sample 1) and Ta(5)/PyCr(5)/[Co$_{88}$Fe$_{12}$(1.3)/ Cu(2.05)]$_8$/Co$_{88}$Fe$_{12}$(1.3)/PyCr(3) (sample 2) were prepared. The numbers in the parentheses indicate the layer thickness in nanometers. The Cu spacer thickness was chosen so that the first sample corresponded to the first GMR maximum and the second sample, to the second maximum. The number of layer pairs (n) was 8 in the first sample and 24 in the second sample. The composite buffer layer Ta(5)/PyCr(5) was used in the first and second samples. Symbol PyCr indicates a permalloy–chromium (Ni$_{80}$Fe$_{20}$)$_{60}$Cr$_{40}$ alloy. The composite structure of sample 2 is shown in Fig. 1a, and a tunneling microscope image of the sample surface is shown in Fig. 1b.

The structures of the samples were analyzed using a DRON_3M diffractometer, CoK_α radiation, and an Si monochromator. The X-ray diffraction patterns of the samples contain the (111) peak of the fcc lattice of Cu and the Co$_{88}$Fe$_{12}$ alloy and oscillations around this peak, which points to high perfection of the layered structure of the samples. An analysis of these data demonstrates that both superlattices have an fcc structure and the axial ⟨111⟩ texture normal to the layer plane.

In addition, we prepared the nanostructure Ta(5.0)/Co$_{88}$Fe$_{12}$(3.5)/Cu(2.0)/Co$_{88}$Fe$_{12}$(3.5)/Ta(5.0) (sample 3), which contained two ferromagnetic Co$_{88}$Fe$_{12}$ layers and a Cu spacer.

The electrical resistances of the samples were measured by the dc four-probe method at room tempera-

ture. The magnetic field and the current were perpendicular to each other and directed in the sample layer plane. The relative magnetoresistance was calculated as $r = [(R(H) - R(0)/R(0)] \times 100\%$, where $R(H)$ is the electrical resistance in field H and $R(0)$ is the zero-field resistance. Figure 2 shows the results of magnetoresistance measurements. Sample 1 has the maximum magnetoresistance (about -44%; see Fig. 2a). The saturation field of this sample determined from the magnetoresistance is about 7.5 kOe. Note that sample 1 exhibits approximately antiparallel ordering of the magnetic moments of neighboring ferromagnetic layers in the absence of an external magnetic field. Sample 2 also has a relatively high magnetization and its saturation is reached in a significantly lower field (about 0.2 kOe). The magnetoresistance of sample 1 is negative and its hysteresis is weak. The magnetoresistance of sample 2, the spacer thickness of which corresponds to the second magnetoresistance maximum, has segments with both negative and positive values and has not hysteresis. Note that the magnetic state in sample 2 with a weak interlayer exchange interaction in a field $H = 0$ is not homogeneous. It is determined by the balance between the energies of local magnetic anisotropy and interlayer exchange interaction and by the presence of structural and magnetic heterogeneities and depends on the history of magnetic state preparation. Figure 2c shows the magnetoresistance dependence of sample 3, which exhibits the maximum hysteresis. When the magnetic field decreases from the saturation field to zero, near-ferromagnetic magnetic ordering is retained in this sample. This means that the energy of the weak interlayer antiferromagnetic exchange interaction is too low to change the magnetic state at $H = 0$. The influence of this interaction on magnetic ordering is strongest in the fields that are equal to the coercive force ($\pm H_c$), at which the mobility of domain walls is highest and they move most intensely. Figure 2d shows the magnetization reversal curve of sample 3. Field $|H_c| = 80 \pm 3$ Oe is seen to coincide with the maxima in the magnetoresistance curve (Fig. 2c). Note that the maximum magnetoresistance of this sample (9.5%) is significantly higher than the typical values of nanostructures of this type ("three-layer" nanostructures).

The passage of electromagnetic waves was studied by the technique described in [31] in the millimeter frequency range 26–38 GHz. A superlattice sample was placed in the cross section of a rectangular waveguide (see Fig. 3a). The relative change in the modulus of transmission coefficient $d_m = [|D(H)| - |D(0)|]/|D(0)|$, where $|D(H)|$ is the modulus of transmission coefficient in field H, was measured. A magnetic field was applied in the superlattice plane parallel to the narrow side of the waveguide, so that dc magnetic field vector $\mathbf{H}$ was perpendicular to the ac magnetic field vector of a wave $\mathbf{h}_\sim$, $\mathbf{H} \perp \mathbf{h}_\sim$.

Microwave spectra of the films were recorded on the equipment of KRTsKP FITs KNTs SO RAN (ELEXSYS E580, Bruker, Germany). The microwave spectra were measured in the X range (resonator pumping frequency was $f = 9.2$ GHz) at room temperature, and a sample was placed in the antinode of the ac magnetic field of a cavity $\mathbf{h}_\sim$. The measurements were carried out when the direction of dc magnetic field $\mathbf{H}$ was changed in both the film plane (in angle φ_H) and the plane parallel to the normal to the film (in angle θ_H; Fig. 3b).

3. RESULTS OF MEASURING THE MICROWAVE GIANT MAGNETORESISTANCE EFFECT AND DISCUSSION

All three samples demonstrate a microwave giant magnetoresistance. Sample 1 exhibits a negative change in the transmission coefficient and a saturation field of 7.3–7.5 kOe, which corresponds to the saturation field of the magnetoresistance curve (see Fig. 4a). The hysteresis of the changes in the transmission coefficient in this sample does not exceed the measurement error; therefore, the curves in Fig. 4a are only plotted for positive magnetic fields. The measurements were performed at several frequencies, and the measured curves are seen to be similar to each other. The curves measured at frequencies of 35 and 38 GHz are slightly different: apart from μGMR, they exhibit FMR-induced resonance changes. The changes in the saturation are 48–53% depending on the frequency, which is comparable with the maximum magnetoresistance (44%) and is slightly higher. Therefore, μGMR and GMR are approximately equal to each other. The results of measuring the microwave transmission in sample 2 are shown in Fig. 4b. Saturation is reached in fields of 0.2–0.25 kOe, which is close to the saturation of the magnetoresistance dependence shown in Fig. 2b. The change in the transmission coefficient at saturation is 24–26%, and the change in the magnetoresistance is about 21%. Figure 4c shows the field dependence of sample 2 recorded at a frequency $f = 26$ GHz and a changed field direction in order to illustrate the microwave transmission hysteresis. The difference between the curves shown in Figs. 2b and 4c consists in the fact that the positive changes in the magnetoresistance reach 2% and the analogous changes at microwaves do not exceed 0.5%. The field range chosen in Fig. 4b to demonstrate the μGMR effect cannot be used to show FMR-induced changes. On the whole, we can conclude that the one-to-one correspondence between GMR and μGMR in the $[\mathrm{Co}_{0.88}\mathrm{Fe}_{0.12}/\mathrm{Cu}]_n$ superlattices, which have the highest magnetoresistance, is only approximate and agrees with the results in [9]. Here, we supplement the data in [9] with the results obtained at various frequencies and focus on the differences between GMR and μGMR.

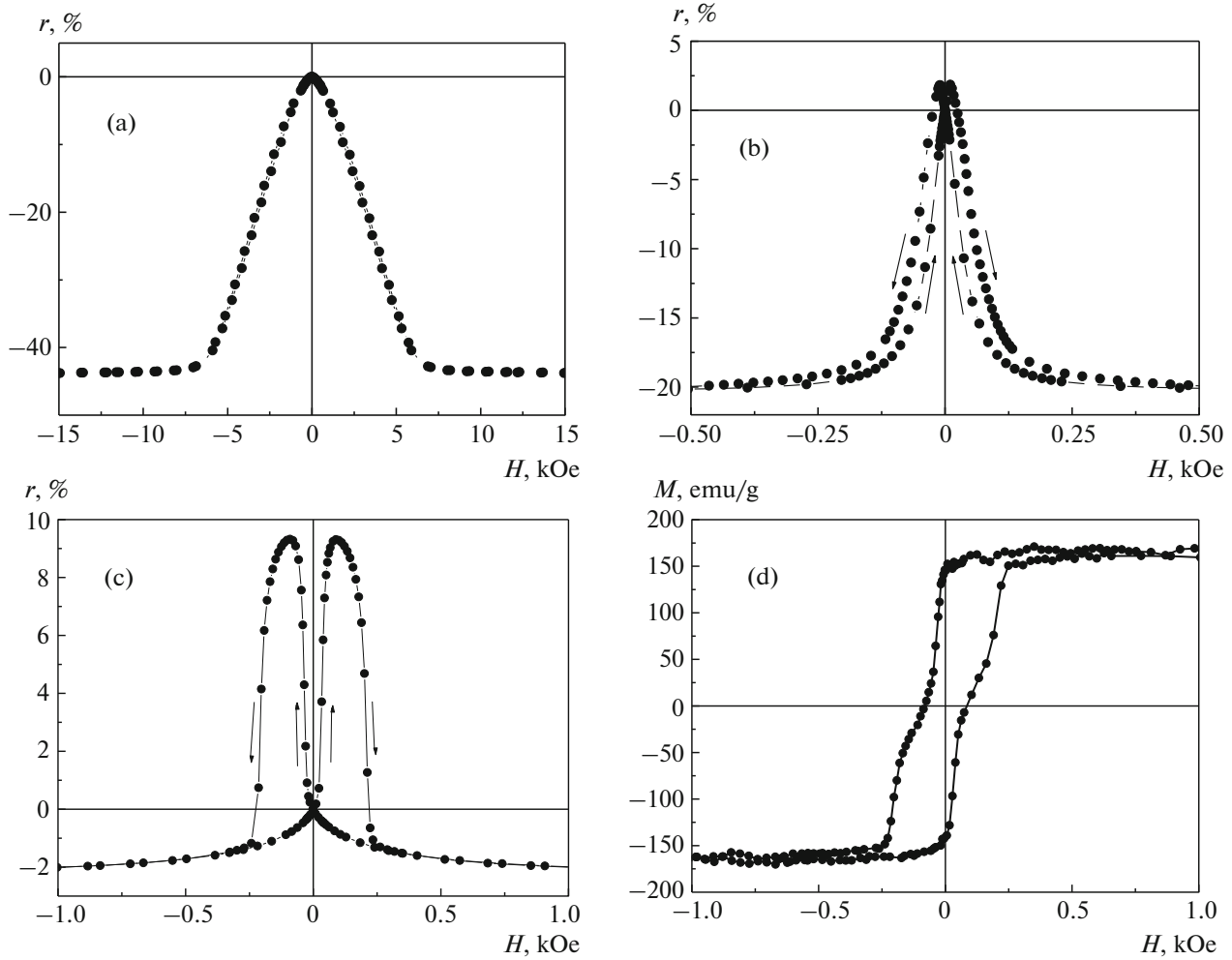The transmission coefficient can be calculated in the simplest manner in the continuous medium

Fig. 2. GMR effect in (a) superlattice sample 1 with a spacer thickness of 0.95 nm, (b) superlattice sample 2 with a spacer thickness of 2.2 nm, (c) three-layer nanostructure sample 3 with a spacer thickness of 2.0 nm, and (d) hysteresis loop of sample 3.

approximation, where a metallic multilayer structure is replaced by a homogeneous plate of the same thickness with an effective electrical conductivity and magnetic susceptibility. In this approximation, we can write the transmission coefficient of an electromagnetic wave D as follows [7]:

$$D = \frac{2Z_m}{2Z_m \cosh k_m d + Z \sinh k_m d}, \qquad (1)$$

where $k_m = (1 + i)/\delta$ is the wavenumber in a conducting medium under normal skin effect conditions, δ is the skin layer thickness, and d is the nanostructure metal thickness (i.e., the total thickness of all metallic layers). The impedance of a well-conducting nanostructure Z_m is lower than the impedance of the waveguide Z, $|Z_m| \ll Z$. We consider Eq. (1) for the limiting case $d \ll \delta$, which takes place at millimeter waves. Then, the transmission coefficient is

$$D = \frac{2Z_m}{Z \sinh k_m d}. \qquad (2)$$

For the typical nanostructure thicknesses (from several to a few hundred nanometers), the inequality $k_m d \ll 1$ is fulfilled and the one-to-one correspondence between the changes in transmission coefficient D and GMR at a direct current, i.e.,

$$d_m = r \qquad (3)$$

takes place.

Equality (3) was repeatedly corroborated in the experiments performed on both nanostructures with continuous layers and layered cluster nanostructures [6, 7, 32–35]. It is fulfilled for the Fe/Cr, Co/Cu, and AgPt/Co superlattices and spin valves [36]. According to Eq. (3), d_m is frequency independent if the frequency dispersion of conductivity is absent. However, some experimental data demonstrate the absence of the one-to-one correspondence between μGMR and GMR. Equality (3) is not fulfilled in granular systems [37] and metallic superlattices in the infrared frequency range [38, 39]. In all cases of deviation from equality (3), the experimentally detected high-fre-
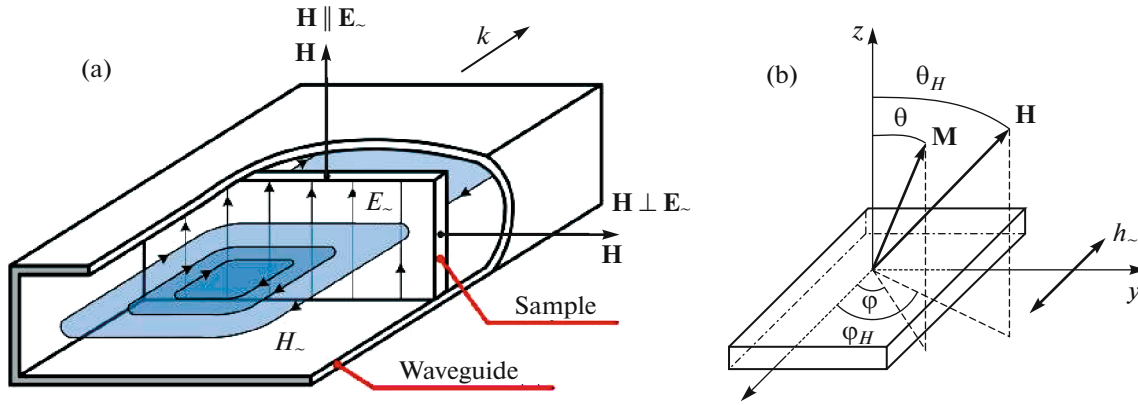
Fig. 3. (Color online) (a) Schematic diagram of microwave transmission measurements and (b) field orientation for experiments in FMR spectrometer.
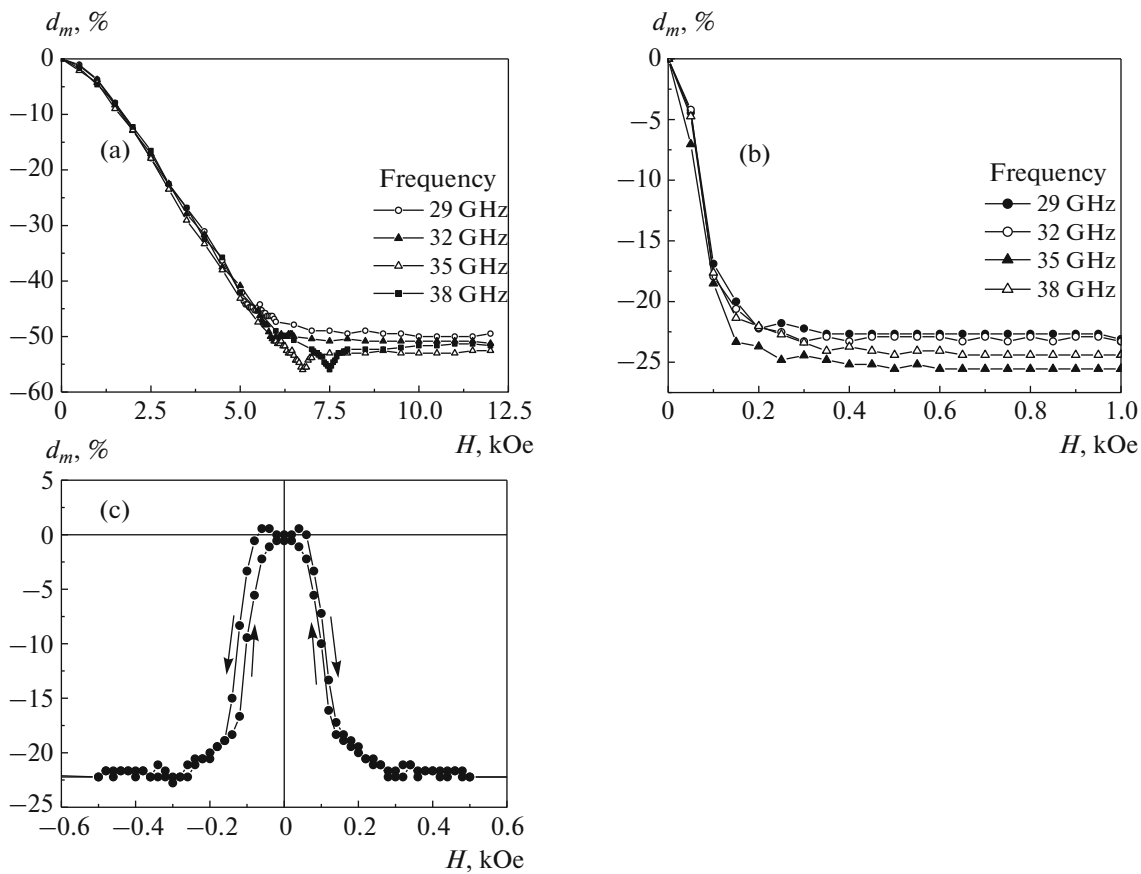

Fig. 4. Microwave GMR effect measured in the superlattices of sample (a) 1 and (b) 2 at several frequencies and (c) the effect measured in sample 2 at a frequency $f = 26$ GHz when the magnetic field direction was changed.

quency μGMR effect was lower than static GMR, $d_m < r$. The frequency dependence of μGMR was comprehensively analyzed in [40, 41]. Deviations from equality (3) in the centimeter and millimeter wavelength ranges were shown to occur in the following two cases: (i) for a very small nanostructure thickness d and (ii) for the effective conductivity that is significantly lower than the typical electrical conductivity of metals. In both cases, the first term in the denominator of Eq. (1) cannot be neglected; therefore, correspondence (3) is not fulfilled toward a lower value of μGMR. In this regard, the results obtained in this work differ from those published earlier. For the $(Co_{0.88}Fe_{0.12})/Cu$ system, we found $d_m > r$.
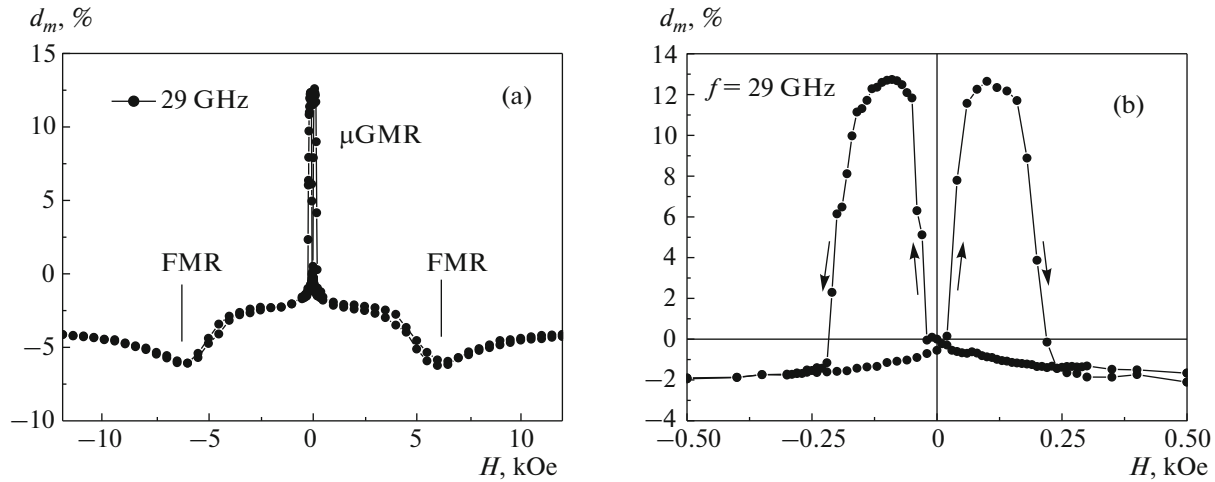
Fig. 5. Microwave GMR effect and FMR in the three-layer structure in the field range (a) ±8 and (b) ±0.5 kOe.

We now consider the results obtained for the three-layer system (sample 3). Figure 5 shows the dependences measured at a frequency f = 29 GHz, and Fig. 5a depicts the dependence obtained in the field range from −8 to +8 kOe. μGMR-induced changes are detected at the fields lower than 0.5 kOe, and a minimum caused by wave absorption under FMR conditions is observed in higher fields near ±6 kOe. Figure 5b shows the dependence measured in the field range from −0.5 to +0.5 kOe; it illustrates the μGMR effect on a larger scale. A qualitative correspondence between GMR in Fig. 2c and μGMR in Fig. 5b is obvious. The dependence in Fig. 5b also has a hysteresis, and the changes in the microwave transmission coefficient are maximal at the fields inducing changes in the magnetoresistance. However, the microwave effect is approximately 30% higher than GMR. The data obtained for the samples under study for comparing GMR and μGMR are given in Table 1.

The detected differences between the static and microwave effects can be caused by the approximate character of Eq. (1) described above. The second cause of these differences can be the transition from Eq. (1) to Eq. (3), which is rigorously valid for the case $r \ll 1$. This second cause seems to be possible for the $[Co_{0.88}Fe_{0.12}/Cu]_n$ superlattices with record GMR, since they are characterized by $r \leq 1$. However, this cause is improper for the three-layer nanostructure

with a lower magnetoresistance ($r \ll 1$). Therefore, the entire set of results can be explained by the first cause, namely, the insufficiency of the effective parameter approximation used to derive Eq. (1).

4. EXCITATION OF EXCHANGE SPIN WAVES IN THIN FERROMAGNETIC FILMS

The type of spin exchange waves—the uniform precession of a magnetization vector experimentally observed during FMR or the standing waves detected by SWR—depends on boundary conditions. The type of pinning is determined by the average magnetic moment at a surface and the magnetization distribution over the film thickness [42]. On the assumption that, in the general case, surface spins are differently (asymmetrically) pinned in different surfaces of a film, the exchange boundary conditions are as follows [18, 25, 26]:

$$\left(\frac{\partial \mathbf{m}}{\partial z} + \beta_1^S \mathbf{m}\right)_{z=d/2} = 0,$$
$$\left(\frac{\partial \mathbf{m}}{\partial z} - \beta_2^S \mathbf{m}\right)_{z=-d/2} = 0,$$

(4)

where $\mathbf{m}$ is the complex amplitude of variable magnetization; β_1^S and β_2^S are the parameters of pinning of surface spins on different film surfaces, which are

Table 1. Comparison of GMR and μGMR

Sample no.	Type of sample	Spacer thickness, nm	Maximum magnetoresistance, %	Maximum change in the transmission coefficient, %
1	Superlattice	0.95	−44	−48...−53
2	Superlattice	2.05	−22	−24...−26
3	Three-layer nanostructure	2.0	+9.3	+12.7

related to the surface anisotropy constant as $\beta^S = K_S/A$; and d is the film thickness, i.e., the total thickness of metallic nanostructure layers in our case.

The pinning parameter of surface spins β^S and surface anisotropy constant K_S can be both positive and negative. At $K_S > 0$ (easy axis of surface anisotropy is normal to the film surface), only harmonic SWR modes with real values of wavevector k are excited. At $K_S < 0$ (hard axis of surface anisotropy is normal to the film surface), a hyperbolic nonpropagating exchange spin wave (surface mode) with an imaginary wavevector is detected apart from harmonic oscillations in an SWR spectrum. The version where two surface modes are detected in an SWR spectrum, which corresponds to the conditions $K_{S1} < 0$ and $K_{S2} < 0$, is also possible. At $K_S = 0$, a homogeneous ac magnetic field $\mathbf{h}_\sim (\mathbf{h}_\sim \perp \mathbf{H})$ only excites a uniform magnetization oscillation $\mathbf{m}_0 \perp \mathbf{M}$ (FMR), since all other possible $m(z)$ oscillations are characterized by a zero dipole moment. In the case of symmetric boundary conditions with $K_S = \infty$, the allowed values of k are $k = \pi n/d$, where n is the trigonometric mode number taking values of 1, 3, 5, 7,... [14].

The resonance field of a uniform mode H_0 at an arbitrary direction of an external magnetic field can be numerically found by solving the set of equations [12, 13, 43]

$$\omega_0 = \frac{\gamma}{M \sin \theta} \left[\frac{\partial^2 E}{\partial \theta^2} \frac{\partial^2 E}{\partial \varphi^2} - \left(\frac{\partial^2 E}{\partial \theta \partial \varphi} \right)^2 \right]^{1/2},$$

$$\frac{\partial E}{\partial \varphi} = \frac{\partial E}{\partial \theta} = 0,$$

$$E = -MH[\sin \theta \sin \theta_H \cos(\varphi - \varphi_H) \qquad (5)$$

$$+ \cos \theta \cos \theta_H] + \frac{K_1}{4}[\sin^4 \theta \sin^2(2\varphi) + \sin^2(2\theta)]$$

$$+ \frac{K_2}{16} \sin^2(2\theta) \sin^2 \theta \sin^2(2\varphi)$$

$$+ [2\pi M^2 + K_n] \cos^2 \theta + K_u \sin^2 \theta \sin^2(\varphi - \varphi_0),$$

where ω_0 is the resonance frequency; $\gamma = 1.758 \times 10^7$ Hz/Oe is the gyromagnetic ratio; E is the total energy of the magnetic system with allowance for the Landau–Lifshitz equation for the motion of magnetization M specified by polar (θ) and azimuth (φ) angles; θ_H and φ_H are the polar and azimuth angles of external magnetizing field H, respectively; K_1 and K_2 are the first and second cubic anisotropy constants, respectively; K_n is the perpendicular uniaxial anisotropy constant; and K_u is the uniaxial anisotropy constant in the plane operating at angle φ_0.

The angular dependence of the nonuniform magnetization eigenmodes (standing exchange spin waves) excited by a homogeneous ac magnetic field $\mathbf{h}_\sim (\mathbf{h}_\sim \perp \mathbf{H})$ at frequency ω is described as follows [44]:

$$\left(\frac{\omega}{\gamma} \right)^2 = \left(H \sin \theta_H + 4\pi M \sin \theta + \frac{2Ak^2}{M} \sin \theta \right)$$

$$\times \left(H \sin \theta_H + \frac{2Ak^2}{M} \sin \theta \right) \qquad (6)$$

$$+ \left(H \cos \theta_H - 4\pi M \cos \theta + \frac{2Ak^2}{M} \cos \theta \right)^2,$$

where A is the intralayer exchange interaction constant. A more complex case of magnetic superlattices, where both bilinear and biquadratic interlayer exchange interactions were taken into account, was considered in [45].

5. RESULTS OF MEASURING FMR AND SWR AND DISCUSSION

FMR and SWR were experimentally studied on sample 2 (Ta(5)/PyCr(5)/[Co$_{88}$Fe$_{12}$(1.3)/Cu(2.05)]$_8$/ Co$_{88}$Fe$_{12}$(1.3)/PyCr(3) superlattice). The total thickness of metallic layers of this superlattice was 26.8 nm. The absorption spectra in the angular range $20°-90°$ are shown in Fig. 6 and the spectra in the range $0°-10°$ are shown in Fig. 7.

Each resonance curve in the angular range $20°-90°$ is identified as the excitation of a uniform mode ($k = 0$). The experimental resonance fields in this angle θ_H range agree well with the curve calculated by solving set (5) (see Fig. 8). Using the dispersion expression for a magnetically isotropic infinite thin disk [46], we find the effective magnetization ($M_{\text{eff}} \approx 1000$ G) provided $\theta = \theta_H = 90°$.

The microwave absorption curves measured in the angular range $0°-10°$, which have a complex shape (Fig. 7), were decomposed into components using a differentiated Lorentz function, the choice of which took into account the absence of contribution of the electric component (because of the cavity design and the sample sizes). Figure 7b shows an example of the performed decomposition.

The modes detected in the microwave spectrum in the angular range $15° < \theta_H < -15°$ were identified as two surface waves (easy plane boundary conditions at $-K_{S1} \neq -K_{S2}$) and a standing exchange spin wave ($n = 1$). An important factor for interpreting the absorption spectra was the mode intensity, which depended on the sample thickness and the magnitude and sign of surface anisotropy constant [17]. When studying the dependence of the ratio of the intensities of the first bulk mode (I_1) to the surface mode (I_S) on the film thickness, the authors of [18] found that $I_S > I_1$ in films thinner than 100 nm and the predominance of I_S over I_1 manifested itself most strongly when a dc magnetic field deviated from the normal to the film.
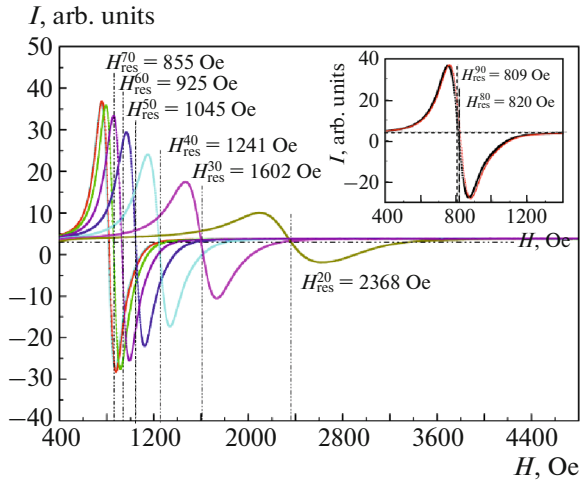
Fig. 6. (Color online) Experimental spectra measured in the angular range 20°–90° (superscript of resonance field indicates angle θ_H).

The dependence of the type of mode (uniform or nonuniform) on angle θ_H was detected even in the first decade after the discovery of SWR [44]. The authors of [44] revealed the angular dependence of resonance fields on angle θ_H (Eq. (6)) and determined the conditions under which the critical angle of transition of nonuniform modes into a uniform mode ($\theta_{H\ \text{critic}}$) can be found. Using Eq. (6), $M_{\text{eff}} \approx 1000$ G, and the conditions described in [44], we calculated $\theta_{H\ \text{critic}}$, which was $15° \pm 2°$ in the field magnetization angle θ range from $0°$ to $25°$. The angle at which the shape of an experimental microwave spectrum becomes composite coincides with $\theta_{H\ \text{critic}}$ (Fig. 8).

The maxima of the surface mode intensities correspond to 4° and 6° [47], which is caused by the deviation of the axis of the uniaxial anisotropy field from the normal to the film by about 5° [48, 49]. The deviation of the axis of the uniaxial anisotropy field can be caused by the $\langle 111 \rangle$ axial texture.

The presence of surface modes in a spectrum makes it possible to determine the surface anisotropy constant. At $K_S < 0$, it is calculated by the formula

$$|K_S| = \left[\frac{M_{\text{eff}} A}{2} \left[(H_S - H_1) - \frac{2A}{M_{\text{eff}}} \left(\frac{\pi}{d} \right)^2 \right] \right]^{1/2}, \quad (7)$$

under symmetric boundary conditions, K_S can be estimated from the expression [50]

$$K_S = \frac{n^2 \pi}{2} \frac{A}{2} \frac{\Delta H_n}{\Delta H_S} \sqrt{\frac{I_n}{I_S}}, \quad (8)$$

where ΔH_n is the linewidth of the nth bulk standing spin wave and ΔH_S is the linewidth of the surface mode.

The simultaneous solution of Eqs. (7) and (8) allows us to estimate A, $|K_{S1}|$, and $|K_{S2}|$ (where $S1$ and $S2$ are the first and second surface modes, respectively) at 0.2×10^{-6} erg/cm, 0.24 erg/cm², and 0.54 erg/cm², respectively. The numerical value of the exchange interaction constant coincides with the data in [51], the authors of which revealed the influence of the ratio of the magnetic and nonmagnetic layer thicknesses on A.

6. CONCLUSIONS

We studied the microwave passage and the ferromagnetic and spin-wave resonances in superlattices
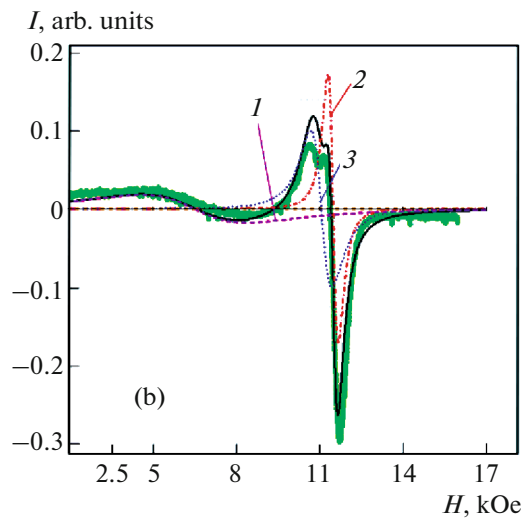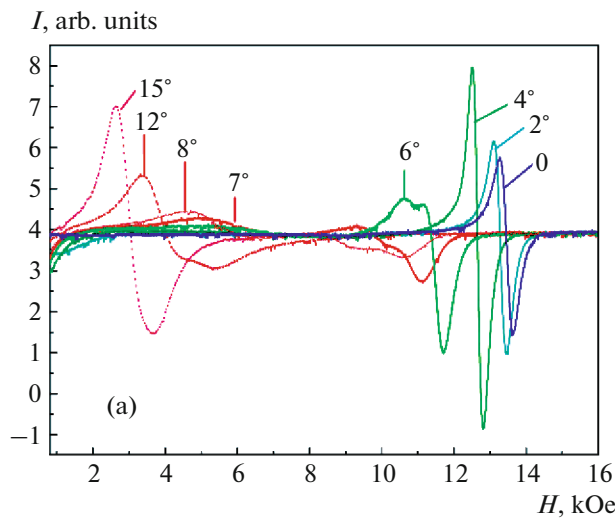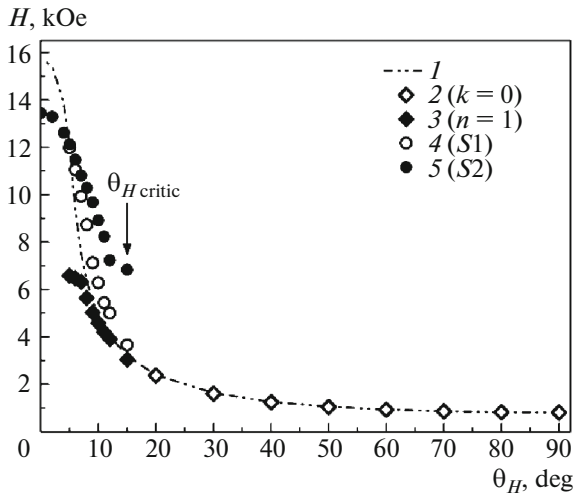

Fig. 7. (Color online) (a) Experimental spectra recorded in the range from 15° to 0°. (b) Example of the decomposition of the experimental spectrum recorded at $\theta_H = 6°$ into Lorentz functions. The numerals in (b) indicate (*1*) the first standing bulk spin mode and (*2, 3*) surface modes.

Fig. 8. Angular dependences of the positions of the resonance fields. Numerals indicate (*1*) fitting curve, (*2*) angular dependence of uniform mode, (*3*) angular dependence of the first standing bulk spin mode, and (*4*, *5*) angular dependences of surface modes.

and a three-layer CoFe/Cu nanostructure. In the frequency range 26−38 GHz, the changes in the coefficient of microwave transmission through CoFe/Cu nanostructures were found to exceed the relative changes in the static magnetoresistance, in contrast to the types of metallic nanostructures studied earlier. This difference is related to the approximation, in which a multilayer nanostructure is replaced by a homogeneous metallic plate the thickness of which is equal to the total thickness of the metallic layers in the nanostructure. An effective conductivity, which includes GMR and effective magnetic susceptibility, is attributed to the plate. For a superlattice with the spacer thickness corresponding to the first GMR maximum, the changes in the microwave transmission coefficient were found to have a giant value, a negative sign, and a very weak hysteresis. For a superlattice with the spacer thickness corresponding to the second GMR maximum, the changes in the microwave transmission coefficient have a high value and both positive and negative signs. The field dependence of the coefficient exhibits a hysteresis. The changes in the coefficient of the three-layer nanostructure reach 12.7% and significantly exceed the static GMR.

The investigation of the dynamic characteristics of the CoFe/Cu multilayer nanostructure demonstrates a uniform distribution of the magnetic parameters over the total sample thickness. The microwave absorption spectra of the nanostructure and their angular dependences allowed us to find the type of boundary conditions (easy plane on either side of pinning standing spin waves irrespective of the angle of a dc magnetic field), to estimate the surface anisotropy constants ($K_{S1} = -0.24$ erg/cm^2, $K_{S2} = -0.54$ erg/cm^2), to detect a devi-

ation of the axis of the uniaxial anisotropy field from the normal to the film, and to find its angular value (approximately 5°).

The formation of nonuniform spin waves for the perpendicular orientation of a film in a dc field allowed us to determine the intralayer exchange interaction constant (0.2×10^{-6} erg/cm). We also found the angle θ_H ranges in which uniform and nonuniform spin waves are excited.

ADDITIONAL INFORMATION

This article was prepared for the special issue dedicated to the centenary of A.S. Borovik-Romanov.

REFERENCES

1. L. A. Prozorova and A. S. Borovik-Romanov, JETP Lett. **10**, 201 (1969).
2. A. S. Borovik-Romanov, *Lectures on Low-Temperature Magnetism. Magnetic Symmetry of Antiferromagnets* (Inst. Fiz. Problem im. P. L. Kapitsy RAN, Moscow, 2010), p. 55 [in Russian].
3. M. N. Baibich, J. M. Broto, A. Fert, et al., Phys. Rev. Lett. **6**, 2472 (1988).
4. G. Binasch, P. Grünberg, F. Saurenbach, and W. Zinn, Phys. Rev. B **39**, 4828 (1989).
5. J. J. Krebs, P. Lubitz, A. Chaiken, and G. A. Prinz, J. Appl. Phys. **69**, 4795 (1991).
6. V. V. Ustinov, A. B. Rinkevich, L. N. Romashev, and V. I. Minin, J. Magn. Magn. Mater. **177−181**, 1205 (1998).
7. A. B. Rinkevich, L. N. Romashev, and V. V. Ustinov, J. Exp. Theor. Phys. **90**, 834 (2000).
8. A. B. Rinkevich, M. A. Milyaev, L. N. Romashev, and D. V. Perov, Phys. Met. Metall. **119**, 1297 (2018).
9. A. B. Rinkevich, Ya. A. Pakhomov, E. A. Kuznetsov, A. S. Klepikova, M. A. Milyaev, L. I. Naumova, and V. V. Ustinov, Tech. Phys. Lett. **45**, 225 (2019).
10. L. Dreher et al., Phys. Rev. B **87**, 224422 (2013).
11. A. Layadi, Phys. Rev. B **66**, 184423 (2002).
12. J. Smith and H. G. Beljers, Philips Res. Rep. **10**, 113 (1955).
13. J. O. Artman, Phys. Rev. **105**, 74 (1957).
14. C. Kittel, Phys. Rev. **110**, 1295 (1958).
15. W. S. Ament and G. T. Rado, Phys. Rev. **97**, 1558 (1955).
16. H. Puszkarski, Prog. Surf. Sci. **9**, 191 (1979).
17. H. Puszkarski and P. Tomczak, Surf. Sci. Rep. **72**, 351 (2017).

18. Yu. A. Korchagin, R. G. Khlebopros, and N. S. Chistyakov, Fiz. Met. Metalloved. **34**, 1303 (1972).

19. A. M. Portis, Appl. Phys. Lett. **2** (4), 69 (1963).

20. E. Schlömann, J. Appl. Phys. **36**, 1193 (1965).

21. R. S. Iskhakov, L. A. Chekanova, and I. G. Vazhenina, Bull. Russ. Acad. Sci.: Phys. **77**, 1265 (2013).

22. V. A. Ignatchenko and D. S. Tsikalov, in *Proceedings of the 6th Euro-Asion Symposium on Trends in MAGnetism, 2016*, p. 264.

23. R. S. Iskhakov, S. V. Stolyar, M. V. Chizhik, and L. A. Chekanova, JETP Lett. **94**, 301 (2011).

24. R. S. Iskhakov, C. V. Stolyar, L. A. Chekanova, and M. V. Chizhik, Phys. Solid State **54**, 748 (2012).

25. Yu. A. Korchagin, R. G. Khlebopros, and N. S. Chistyakov, Sov. Phys. Solid State **14**, 1826 (1972).

26. N. M. Salanskii and M. Sh. Erukhimov, *Physical Properties and Application of Magnetic Films* (Nauka, Novosibirsk, 1975) [in Russian].

27. A. G. Gurevich, *Magnetic Resonance in Ferrites and Antiferromagnetics* (Nauka, Moscow, 1973) [in Russian].

28. V. M. Sokolov and B. A. Tavger, Sov. Phys. Solid State **10**, 1412 (1968).

29. N. S. Bannikova, M. A. Milyaev, L. I. Naumova, V. V. Proglyado, T. P. Krinitsina, I. Yu. Kamenskii, and V. V. Ustinov, Phys. Met. Metallogr. **116**, 987 (2015).

30. N. S. Bannikova, M. A. Milyaev, L. I. Naumova, E. I. Patrakov, V. V. Proglyado, I. Yu. Kamenskii, M. V. Ryabukhina, and V. V. Ustinov, Phys. Met. Metallogr. **119**, 1073 (2018).

31. A. B. Rinkevich, M. I. Samoilovich, S. M. Klescheva, D. V. Perov, A. M. Burkhanov, and E. A. Kuznetsov, IEEE Trans. Nanotechnol. **13**, 3 (2014).

32. T. Rausch, T. Szczurek, and M. Schlesinger, J. Appl. Phys. **85**, 314 (1999).

33. A. Rinkevich, L. Romashev, M. Milyaev, E. Kuztetsov, M. Angelakeris, and P. Poulopoulos, J. Magn. Magn. Mater. **317**, 15 (2007).

34. V. V. Ustinov, A. B. Rinkevich, L. N. Romashev, M. A. Milyaev, A. M. Burkhanov, N. N. Sidun, and E. A. Kuznetsov, Phys. Met. Metallogr. **99**, 486 (2005).

35. D. P. Belozorov, V. N. Derkach, S. V. Nedukh, A. G. Ravlik, S. T. Roschenko, I. G. Shipkova, S. I. Tarapov, and F. Yildiz, Int. J. Infrared Millimeter Waves **22**, 1669 (2001).

36. D. E. Endean, J. N. Heyman, S. Maat, and E. Dan Dahlberg, Phys. Rev. **84**, 212405 (2011).

37. A. B. Granovsky, A. A. Kozlov, T. V. Bagmut, S. V. Nedukh, S. I. Tarapov, and J. P. Clerc, Phys. Solid State **47**, 738 (2005).

38. J. C. Jackuet and T. Valet, in *Proceedings of the Mater. Res. Soc. Symposium on Magnetic Ultrathin Films, Multilayers and Surfaces, USA, San Francisco, 1995*, MRS Symp. Proc. 384, 477 (1995).

39. I. D. Lobov, M. M. Kirillova, L. N. Romashev, M. A. Milyaev, and V. V. Ustinov, Phys. Solid State **51**, 2480 (2009).

40. V. V. Ustinov, A. B. Rinkevich, L. N. Romashev, A. M. Burkhanov, and E. A. Kuznetsov, Phys. Met. Metallogr. **96**, 291 (2003).

41. D. V. Perov and A. B. Rinkevich, Phys. Met. Metallogr. **120**, 333 (2019).

42. J. T. Yu, R. A. Turk, and P. E. Wigen, Phys. Rev. B **11**, 420 (1975).

43. H. Suhl, Phys. Rev. **97**, 555 (1955).

44. P. E. Wigen, C. F. Kooi, M. R. Shanabarger, U. K. Cummings, and M. E. Baldwin, J. Appl. Phys. **34**, 1137 (1963).

45. A. B. Drovosekov, O. V. Zhotikova, N. M. Kreines, V. F. Meshcheryakov, M. A. Milyaev, L. N. Romashev, V. V. Ustinov, and D. I. Kholin, J. Exp. Theor. Phys. **89**, 986 (1999).

46. C. Kittel, Phys. Rev. **73**, 155 (1948).

47. I. G. Vazhenina, R. S. Iskhakov, M. V. Rautskii, M. A. Milyaev, and L. I. Naumova, Phys. Solid State **62**, 153 (2020).

48. A. Layadi, Phys. Rev. B **63**, 174410 (2001).

49. J. A. Hagmann, K. Traudt, Y. Y. Zhou, X. Liu, M. Dobrowolska, and J. K. Furdyna, J. Magn. Magn. Mater. **360**, 137 (2014).

50. A. Stankov, in *Proceedings of the International Symposium on Physics of Magnetic Films* (1968), p. 422.

51. R. S. Iskhakov, N. A. Shepeta, S. V. Stolyar, L. A. Chekanova, and V. Yu. Yakovchuk, JETP Lett. **83**, 28 (2006).

Translated by K. Shakhlevich